ELSEVIER

PII: S0955-2219(97)00029-0

Journal of the European Ceramic Society 17 (1997) 1597–1612

0955-2219/97/$17.00

Wear Resistance of Crystals of Corundum Doped with Cr_2O_3, TiO_2, and CoO

Janusz J. Partyka

Department of Refractory, Fine and Technical Ceramics, Faculty of Material Science and Ceramics, University of Mining and Metallurgy, Cracow, Poland

(Received 13 June 1996; accepted 10 February 1997)

Abstract

The wear resistance of crystals of corundum sliding on cast iron was determined as a function of crystallographic orientation with respect to the plane of wear and rubbing direction and as a function of changes of structure of crystals. The experimental work was based on Verneuil grown single crystals of synthetic corundum (α-Al_2O_3); non-doped and doped with: Cr_2O_3 amount 0·5 and 1·5% wt.; TiO_2 amount 0·1 and 0·25% wt.; CoO amount 0·1 and 0·5% wt.. Wear resistance (as an inverse of abrasion wear) *was determined on four crystallographic planes: (0001); $\{11\bar{2}0\}$; $\{11\bar{2}\cdot 12\}$; $\{11\bar{2}3\}$ and twelve rubbing directions, started from [1100] direction, every 30°. A varying sliding rate of the specimens of the crystals over the surface of the cylinder of cast iron was used. The orientation of the specimens was determined by standard Laue techniques, and after this, was checked by X-ray-line-reflection techniques* (simultaneously the $[\bar{1}100]$ direction was determined). *The volume of material lost by wear from the surface of crystals was calculated from the change of the planimetred profile of the surface (before and after wear) of two perpendicular outlines of specimens.* © *1997 Elsevier Science Limited.*

1 Introduction

Mono-corundum, used in the abrasive material industry, constitutes one form of aluminium oxide grain. Its method of production was firstly formulated by Hoglund. Mono-corundum grains, produced on a full-scale basis, are fine and highly broken-down; they raise serious difficulties in terms of evaluating the crystallographic orientation. With regard to such difficulties and the anisotropy of the properties of corundum the present research uses corundum single crystals obtained by Verneuille's method as a model for mono-corundum grain. The corundum single crystals, obtained by this method, are characterised by a highly defected crystals lattice similar to that of mono-corundum and by the presence of internal stresses; however, there is the possibility of orientation.

2 Experimental

In the present study, single crystals of corundum α-Al_2O_3 (obtained by the method of Verneuille's) doped with chromium, titanium and cobalt were used:

(1) Cr_2O_3 in the amount:0·5 wt%(denoted K-1)
1.5 wt%(denoted K-2);
(2) TiO_2 in the amount:0·1 wt%(denoted K-3)
0·25 wt%(denoted K-4);
(3) CoO in the amount:0·1 wt%(denoted K-5)
0·5 wt%(denoted K-6);

and for the sake of comparison a non-doped ('pure') crystal of corundum(denoted K-0)

In order to determine the effect of doping on the abrasive resistance of corundum crystals, their hardness and behaviour in the process of continuous grinding were examined. There was also determined the effect of doping on the basic structural parameters on the basis of the following measurements:

(1) the real content of dopant (chemical analysis and spectral analysis) — Table 1;
(2) optical absorption (before and after annealing in oxygen atmosphere at 1500°C) — Table 2;
(3) electrical conductivity (at 1500°C depend from different partial pressure of the oxygen) — Table 3;

Table 1. Determination of amounts of the dopants and impurities in corundum crystals

Crystal	*Analysis type*	Cr_2O_3	TiO_2	CoO	SiO_2	Fe_2O_3	CaO	MgO	K_2O	Na_2O
K-O	spectral	+	+	—	+	+ +	+	—	—	—
	chemical	—	—	—	—	0·012	—	—	0·04	0·025
K-1	spectral	+ +	+	—	+	+ +	—	—	—	—
	chemical	0·413	—	—	—	0·018	—	—	0·06	0·033
K-2	spectral	+ +	+	+	+	+ +	+	+	—	—
	chemical	1·278	—	—	—	0·019	—	—	0·01	0·022
K-3	spectral	+ +	—	—	—	+ +	—	—	—	—
	chemical	—	0·069	—	—	—	—	—	—	0·029
K-4	spectral	+	+ +	—	+	+ +	—	—	—	—
	chemical	—	0·153	—	—	0.012	—	—	—	0·029
K-5	spectral	+	+	+ +	—	+ +	+	—	—	—
	chemical	—	—	0·08	—	0·0096	—	—	0·02	0·044
K-6	spectral	+	+	+ +	—	+ +	+	—	—	—
	chemical	—	—	0·22	—	0·022	—	—	0·03	0·053

+ + occur in trace, + + occur, — don't occur.

Table 2. Optical absorption of the corundum crystals (peak of optical absorption, in [nm])

Measurement plane	*K-1*	*K-2*	*K-3*	*K-4*	*K-5*	*K-6*
(0001)	*550 ; 470*	*570 ; 550*	*560 ; 490*	*570 ÷ 670*	*640 ; 470*	*640 ; 540*
	400 ; 380	*470 ; 400*		*500*	*430*	*470 ; 440*
		370				
	570 ; 550	**570 ; 550**	**560 ; 480**	**570 ; 480**	**640 ; 530**	**640 ; 540**
	470 ; 380	**470 ; 400**			**430**	**430**
{11$\bar{2}$0}	*550 ; 500*	*570 ; 550*	*560 ; 490*	*570 ; 500*	*650 ; 470*	*640 ; 470*
	400	*470 ; 400*			*430*	*430*
		370				
	570 ; 550	**550 ; 470**	**560 ; 480**	**570 ; 480**	**650 ; 440**	**640 ; 540**
	470 ; 400	**400 ; 370**				**430**
{11$\bar{2}$·12}	*550 ; 470*	*550 ; 470*	*570*	*570 ; 500*	*640 ; 430*	*640 ; 540*
	400	*400 ; 370*				
{11$\bar{2}$3}	*550 ; 470*	*550 ; 470*	*570*	*570 ; 500*	*640 ; 430*	*640 ; 540*
	400	*400 ; 370*				

Italic numbers — before annealing of the crystals.
Bold numbers — after annealing in oxygen atmosphere at 1500°C

(4) lattice constants of an elementary cell — Table 4;
(5) density of the crystals (evaluated from X-ray analysis and measured) — Table 5;
(6) approximate values of density of the dislocation — Table 6.

The hardness of the crystals was determined using the microhardness tester PMT type, employing Vickers pyramid at a load of 100 G (Fig. 3–4). The abrasive resistance of the crystals was determined as a function of abrasive wear in process of continuous grinding of an oriented grain (a rectangular prism 2 × 2 × 7 mm, cut out from a large oriented crystal) over the surface of a cylinder of cast iron (Fig. 1).

The rate of abrasive wear has been presented in the form of volumetric wear of crystals (V_z) per unit of the abrasion path, determined by means of double planimetrizing (before and after grinding) of the grain in two projections perpendicular to each other (Fig. 2) and calculated according to the relation:

$$V_z = \frac{(F_1 + F_2)(h_1 + h_2)}{4S} [m^3/m]$$

where:

F_1, F_2 — denote the surface abrasive wear of the grain, planimetrized before and after grinding, in two projections (perpendicular to each other).

h_1, h_2 — denote the linear wear of the grain, planimetrized before and after grinding, in two projections (perpendicular to each other).

S — denote the abrasion path.

The measurements of abrasion were carried out at constant loading: 1 kg mm^{-2} of the grain and the same abrasion path; 500 m, varying the crystallographic planes: (0001); {11$\bar{2}$0}; ,{11$\bar{2}$·12}; {11$\bar{2}$3} and varying the crystallographic directions

Table 3. Electrical conductivity of non-doped end doped corundum crystals

Oxygen partial pressure P_{O_2} [MPa]	*Crystallographic plane*	*Electrical conductivity of corundum crystals [Ω^{-1} cm^{-1}]* *K-0*	*K-1*	*K-2*	*K-3*	*K-4*	*K-5*	*K-6*
10^{-8}	(0001)	$4{\cdot}50\ 10^{-8}$	$1{\cdot}62\ 10^{-7}$	$2{\cdot}02\ 10^{-7}$	$8{\cdot}80\ 10^{-7}$	$6{\cdot}02\ 10^{-6}$	$5{\cdot}60\ 10^{-6}$	$4{\cdot}52\ 10^{-5}$
	$\{11\bar{2}0\}$	$4{\cdot}16\ 10^{-8}$	$1{\cdot}01\ 10^{-7}$	$1{\cdot}96\ 10^{-7}$	$2{\cdot}06\ 10^{-6}$	$5{\cdot}34\ 10^{-6}$	$1{\cdot}03\ 10^{-5}$	$4{\cdot}09\ 10^{-5}$
	$\{11\bar{2} \cdot 12\}$	$9{\cdot}88\ 10^{-9}$	$6{\cdot}12\ 10^{-8}$	$8{\cdot}34\ 10^{-8}$	$9{\cdot}54\ 10^{-7}$	$2{\cdot}07\ 10^{-6}$	$7{\cdot}10\ 10^{-7}$	$7{\cdot}54\ 10^{-6}$
	$\{11\bar{2}3\}$	$2{\cdot}64\ 10^{-8}$	$5{\cdot}34\ 10^{-8}$	$8{\cdot}12\ 10^{-8}$	$9{\cdot}06\ 10^{-7}$	$9{\cdot}94\ 10^{-7}$	$2{\cdot}40\ 10^{-6}$	$4{\cdot}55\ 10^{-6}$
10^{-5}	(0001)	$7{\cdot}95\ 10^{-8}$	$2{\cdot}60\ 10^{-7}$	$2{\cdot}50\ 10^{-7}$	$1{\cdot}91\ 10^{-7}$	$4{\cdot}00\ 10^{-6}$	$9{\cdot}07\ 10^{-6}$	$2{\cdot}00\ 10^{-5}$
	$\{11\bar{2}0\}$	$7{\cdot}92\ 10^{-8}$	$2{\cdot}28\ 10^{-7}$	$3{\cdot}00\ 10^{-7}$	$9{\cdot}89\ 10^{-7}$	$1{\cdot}22\ 10^{-6}$	$8{\cdot}43\ 10^{-6}$	$1{\cdot}36\ 10^{-5}$
	$\{11\bar{2} \cdot 12\}$	$4{\cdot}12\ 10^{-8}$	$8{\cdot}29\ 10^{-8}$	$4{\cdot}40\ 10^{-8}$	$6{\cdot}66\ 10^{-7}$	$8{\cdot}07\ 10^{-7}$	$8{\cdot}52\ 10^{-6}$	$6{\cdot}86\ 10^{-6}$
	$\{11\bar{2}3\}$	$5{\cdot}02\ 10^{-8}$	$8{\cdot}00\ 10^{-8}$	$1{\cdot}21\ 10^{-7}$	$6{\cdot}60\ 10^{-7}$	$7{\cdot}15\ 10^{-7}$	$1{\cdot}23\ 10^{-6}$	$5{\cdot}94\ 10^{-6}$
0·02	(0001)	$6{\cdot}63\ 10^{-7}$	$6{\cdot}88\ 10^{-7}$	$8{\cdot}15\ 10^{-7}$	$2{\cdot}50\ 10^{-7}$	$6{\cdot}50\ 10^{-6}$	$9{\cdot}82\ 10^{-6}$	$4{\cdot}03\ 10^{-5}$
	$\{11\bar{2}0\}$	$5{\cdot}40\ 10^{-7}$	$6{\cdot}87\ 10^{-7}$	$7{\cdot}18\ 10^{-7}$	$5{\cdot}75\ 10^{-6}$	$5{\cdot}35\ 10^{-6}$	$3{\cdot}27\ 10^{-5}$	$5{\cdot}13\ 10^{-5}$
	$\{11\bar{2} \cdot 12\}$	$5{\cdot}27\ 10^{-8}$	$7{\cdot}56\ 10^{-8}$	$4{\cdot}54\ 10^{-7}$	$9{\cdot}83\ 10^{-7}$	$2{\cdot}21\ 10^{-6}$	$1{\cdot}63\ 10^{-5}$	$8{\cdot}12\ 10^{-5}$
	$\{11\bar{2}3\}$	$8{\cdot}42\ 10^{-7}$	$9{\cdot}02\ 10^{-8}$	$3{\cdot}86\ 10^{-7}$	$4{\cdot}40\ 10^{-7}$	$2{\cdot}03\ 10^{-6}$	$3{\cdot}40\ 10^{-6}$	$7{\cdot}05\ 10^{-6}$
0·1	(0001)	$4{\cdot}20\ 10^{-7}$	$9{\cdot}01\ 10^{-7}$	$1{\cdot}20\ 10^{-6}$	$2{\cdot}53\ 10^{-6}$	$8{\cdot}10\ 10^{-6}$	$1{\cdot}07\ 10^{-5}$	$1{\cdot}00\ 10^{-4}$
	$\{11\bar{2}0\}$	$3{\cdot}60\ 10^{-7}$	$8{\cdot}89\ 10^{-7}$	$9{\cdot}97\ 10^{-7}$	$3{\cdot}17\ 10^{-5}$	$8{\cdot}87\ 10^{-5}$	$5{\cdot}66\ 10^{-5}$	$1{\cdot}02\ 10^{-4}$
	$\{112 \cdot 12\}$	$9{\cdot}41\ 10^{-8}$	$1{\cdot}02\ 10^{-7}$	$6{\cdot}33\ 10^{-7}$	$9{\cdot}89\ 10^{-7}$	$3{\cdot}42\ 10^{-6}$	$3{\cdot}04\ 10^{-5}$	$1{\cdot}94\ 10^{-5}$
	$\{11\bar{2}3\}$	$6{\cdot}34\ 10^{-7}$	$1{\cdot}00\ 10^{-7}$	$6{\cdot}02\ 10^{-7}$	$1{\cdot}05\ 10^{-6}$	$3{\cdot}17\ 10^{-6}$	$3{\cdot}22\ 10^{-5}$	$9{\cdot}07\ 10^{-6}$

Table 4. Values of the lattice constants of an elementary cell of the corundum crystals

Parameter	*K-0*	*K-1*	*K-2*	*K-3*	*K-4*	*K-5*	*K-6*
a [A]	4·7426	4·7519	4·7543	4·7569	4·7577	4·7508	4·7543
Δa [A]	−0·0165	0·0093	0·0117	0·0443	0·0151	0·0082	0·0117
c [A]	12·9660	12·9795	12·9761	12·9501	13·0066	12·9701	12·9954
Δc [A]	−0·0234	0·0101	0·0235	−0·0159	0·0406	0·0041	0·0294
V [A^2]	252·923	253·824	254·205	253·774	254·974	253·516	254·381
ΔV [A^2]	−1·857	0·901	1·202	0·851	2·051	0·953	1·458

($a_o = 4{\cdot}7591$ A; $c_o = 12{\cdot}9894$ A; $V_o = 254{\cdot}78\ 10^{-28}$ cm^3 *Handbook of Chemistry and Physics.* CRC-Press).

Table 5. Density of corundum crystals (evaluated from X-ray analysis and measured)

Density [g cm^{-3}]	*K-0*	*K-1*	*K-2*	*K-3*	*K-4*	*K-5*	*K-6*
ρ evaluat.	4·0213	4·0068 (−0·0245)	4·0153 (−0·0060)	(1) 4·0042 (−0·0171) (2) 4·0030 (−0·0183) (3) 4·0113 (−0·0100) (4) 4·0063 (−0·0150)	(1) 3·9842 (−0·0371) (2) 3·9853 (−0·0360) (3) 3·9867 (−0·0346) (4) 3·9946 (−0·0267)	(1) 4·0084 (−0·0129) (2) 4·0119 (−0·0094)	(1) 3·9982 (−0·0231) (2) 4·0071 (−0·0142)
ρ measur.	4·0289	4·0142 (−0·0147)	4·0237 (−0·0052)	4·0178 (−0·0111)	4·0049 (−0·0240)	4·0096 (−0·0193)	4·0014 (−0·0275)

(1); (2); (3); (4) — mean, taken pattern of solve of the dopants: (*in brackets*) — difference between density of pure and dopened

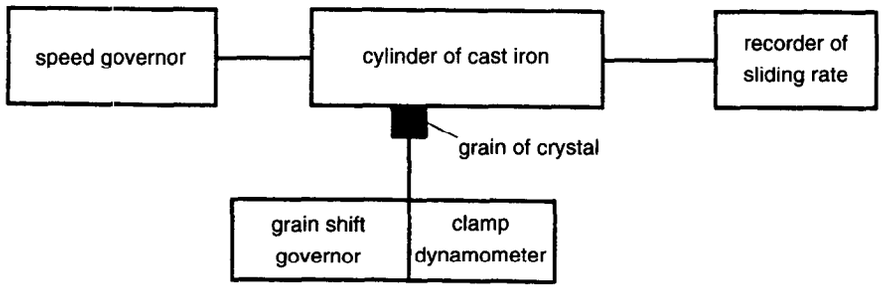

Fig. 1. Block diagram of the measurement system of abrasive wear.

Table 6. Approximate values of density of the dislocation of the corundum crystals [lines cm^{-2}] (evaluated from X-ray measurements)

Measurement plane	*K-0*	*K-1*	*K-2*	*K-3*	*K-4*	*K-5*	*K-6*
(0001)	$2.89\ 10^7$	$7.69\ 10^6$	$8.26\ 10^6$	$1.42\ 10^7$	$2.39\ 10^7$	$9.51\ 10^6$	$1.15\ 10^7$
$\{11\bar{2}0\}$	$1.69\ 10^7$	$7.25\ 10^6$	$9.21\ 10^6$	$8.44\ 10^6$	$9.32\ 10^6$	$6.03\ 10^6$	$8.37\ 10^6$
$\{11\bar{2}\cdot 12\}$	$5.90\ 10^5$	$8.38\ 10^4$	$1.13\ 10^5$	$5.65\ 10^5$	$6.09\ 10^5$	$7.08\ 10^4$	$8.42\ 10^4$
$\{11\bar{2}3\}$	$5.94\ 10^5$	$7.59\ 10^4$	$2.56\ 10^5$	$6.02\ 10^5$	$6.26\ 10^5$	$9.84\ 10^4$	$1.53\ 10^5$

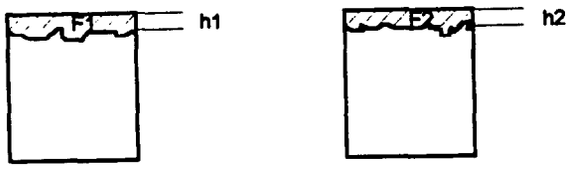

Fig. 2. Planimetrizing system of perpendicular projections before and after wear.

of abrasion: starting from the direction $[\bar{1}100]$ and changing direction every 30° around the circumference of a circle, and varying the sliding ratio 1·6; 3·2; 6·4; 12·5 and 25 m s^{-1}. The results of abrasion wear (volumetric wear of crystals per unit of the abrasion wear [$m^3\,m^{-1}$] in logarithmic scale) are shown in Figs 5–24 (all for the crystallographic planes (0001); $\{11\bar{2}0\}$ and some selected for the planes $\{11\bar{2}\cdot 12\}$; $\{11\bar{2}3\}$.

Additionally, to verify the hypothesis about the influence of the dopant on the mechanical properties of corundum single crystals calculations were carried out concerning: the linear correlations between two variables by the last square method; the significance of linear correlations between abrasive wear (for abrasive wear the value V_z was selected for three abrasion directions 90; 180 and 270° at three abrasions rates: 3·2; 6·4 and 12·5 m s^{-1}) and the real density; the dislocation density on the particular planes of the examined crystals.

3 Discussion

During the formation of corundum single crystals the volatilisation of a part of the dopant was observed which suggests the necessity to determine the part of the dopant retained in a monocrystalline block during the production process of monocorundum under industrial conditions. The presence of dopant leads to the creation of different defects in the crystals.

3.1 Cr-doped corundum crystals

The dopant of chromium (chiefly Cr^{+3}) in corundum crystals substitutes for the ion Al^{+3}, generally

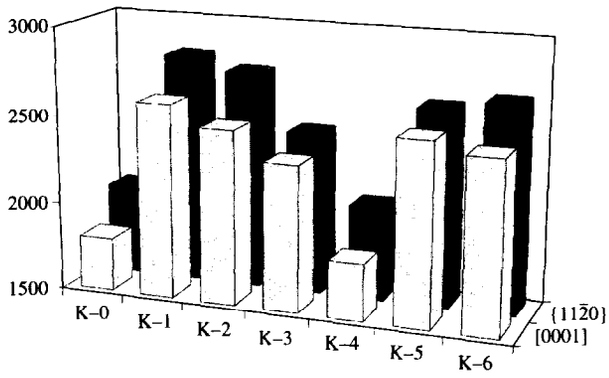

Fig. 3. Microhardness of corundum crystals measured on crystallographic planes (0001) and $\{11\bar{2}0\}$.

without producing any other defects. It becomes uniformly distributed close to the examined surfaces, and in comparison with non-doped corundum crystals, it contributes to the formation of crystals with mosaic blocks of greater dimensions and lower values of the dislocation density.

As a dopant in corundum, chromium causes considerable hardening by doping, based on the mechanism of solid-solution hardening, which is especially noticeable at the content 0·5 wt% of Cr_2O_3, at which the most advantageous mechanical properties have been obtained (increasing abrasion resistance, microhardness). On the other hand, a higher content of chromium; 1·5 wt% of Cr_2O_3 induces a marked deformation of the lattice, caused by the difference in the ionic radii $Cr^{+3(+2)}$ and Al^{+3}, and by the appearance of a part of the dopant in the form of microprecipitations which are manifested by an increase in the dislocation density, by the occurrence of finer mosaic blocks and, as a consequence, by a deterioration in the mechanical properties.

The lattice deformation of corundum crystals doped by chromium ions arises from the following incorporation reaction:

$$xCr_2O_3 + (1-x)Al_2O_3 \leftrightarrow Al_{2-2x}Cr_{2x}O_3$$

3.2 Ti-doped corundum crystals

The dopant titanium (chiefly Ti^{+4} and small amounts of Ti^{+3}) in corundum crystals substitutes

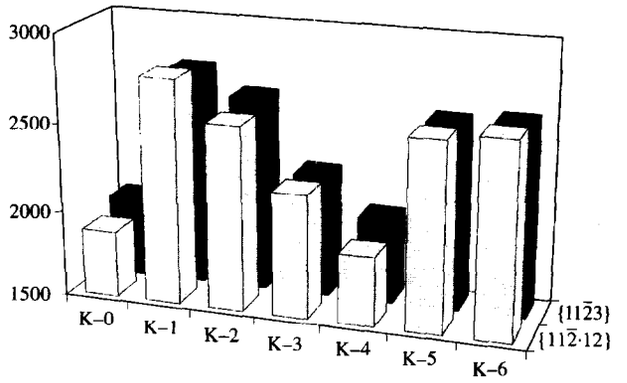

Fig. 4. Microhardness of corundum crystals measured on crystallographic planes {11$\bar{2}$·12} and {11$\bar{2}$3}.

for the ion Al^{+3}, which induces the occurrence of additional defects: Al vacancies (V_{Al}) and/or oxygen interstitial ions, O^{-2}. Because of considerable differences in ionic radii between $Ti^{+4(+3)}$ and Al^{+3}, deformed crystals are formed with considerable internal stresses, and with dislocation density values and the magnitude of the mosaic blocks not much different from the corresponding values in non-doped corundum crystals.

The dopant titanium in the amount 0·1 wt% of TiO_2 produces the effect of hardening by doping, based on the mechanism of solid-solution hardening. An increase in TiO_2 content up to 0·25 wt% resulted in considerable worsening of the examined mechanical properties to values comparable with those obtained for non-doped corundum crystals.

The proposed models of the lattice deformation of the corundum crystals doped by titanium ions:

(1) for Ti^{+3}–$3xTiO_2 + (1-x)Al_2O_3 \leftrightarrow Al_{2-2x}Ti_{3x}O_3$;
(2) for Ti^{+4} — with Al vacancies $3xTiO_2 + (1-2x)Al_2O_3 \leftrightarrow Al_{2-4x}Ti_{3x}O_3 + V_{Al}$;
(3) for Ti^{+4} — with interstitial ions O^{-2} — $2xTiO_2 + (1-x)Al_2O_3 \leftrightarrow Al_{2-2x}Ti_{2x}O_{3-x}$;
(4) for Ti^{+4} — with vacancies Al and interstitial ions O^{-2} —$xTiO_2 + (1-x)Al_2O_3 \leftrightarrow Al_{2-2x}Ti_xO_{3-x} + xV_{Al} + xV_O$.

3.3 Co-doped corundum crystals

The dopant of cobalt (Co^{+3} and Co^{+2}) in corundum crystals substitutes mainly for the Al^{+3} ions with the following results:

(1) in the case of Co^{+3} it does not produce any additional defects;
(2) in the case of Co^{+2} it causes additional formation of the vacancy O(V_O).

The presence of Co^{+2} ion of a great ionic radius causes considerable 'swelling' of the structure of corundum and the occurrence of stresses. Besides this it is responsible for a decrease in the dislocation density and for the formation of the largest (among the examined crystals) mosaic blocks.

Similary, as for chromium, cobalt induces considerable hardening by doping, based on the mechanism of solid-solution hardening at the content 0·1 wt% of CoO; at the content 0·5 wt% of CoO distinct changes in the mechanical properties were not observed in spite of great 'swelling' of the structure. This suggests that besides the mentioned mechanism of solid-solution hardening the mechanism of precipitation hardening begins to interact.

The proposed model of the lattice deformation of the corundum crystals doped by cobalt ions:

(1) for Co^{+2} — with vacancies O — $2xCoO + (1-x)Al_2O_3 \leftrightarrow Al_{2-2x}Co_{2x}O_{3-x} + xV_O$;
(2) *for Co^{3+} — $3xCoO_3 + (1-x)Al_2O_3 \leftrightarrow Al_{2-2x}Co_{3x}O_3$.

Application of chromium, titanium and cobalt dopants in the production of modified mono-corundum crystals will be advantageous on account of the marked improvement of the mechanical properties of corundum crystals (abrasion resistance, microhardness).

The dopants chromium and cobalt have a particulary advantageous effect, while titanium gives this effect only up to the content 0·1 wt% of TiO_2. All dopants additionally caused an increase in the brittleness of the monocrystals which should have an advantageous effect on the self-sharpening ability of mono-corundum.

The examined samples revealed distinct anisotropy of the properties depending on the crystallographic plane and the direction of abrasion. Very good results (high microhardness and abrasive resistance) were obtained on the crystallographic planes basic (0001) and prismatic {11$\bar{2}$0}, which are especially advantageous as these planes occur in a natural way on the corundum surface.

An analysis of correlations between abrasive wear and densities of crystals (as a function of lattice deformation) and between abrasive wear and dislocation density has shown that there exists a linear correlation between these parameters for all dopants on the basic (0001) and on the prismatic {11$\bar{2}$0} planes. On the remaining planes a correlation has been found for the dopant cobalt (on the planes {11$\bar{2}$ · 12}; {11$\bar{2}$3} and chromium (on the plane {11$\bar{2}$ · 12}).

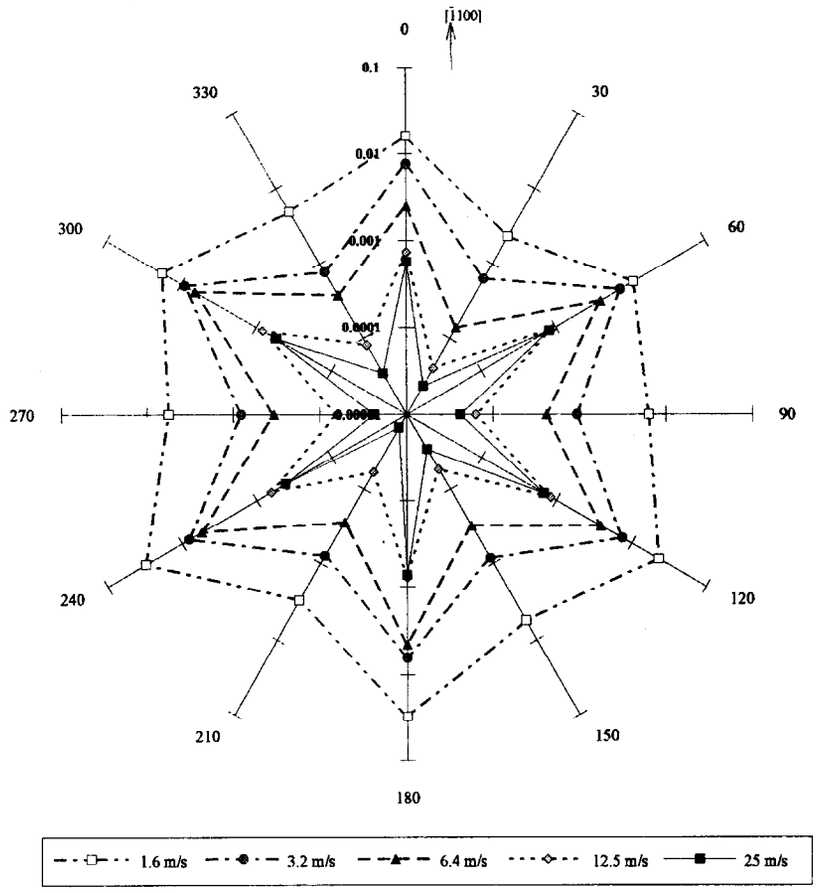

Fig. 5. Abrasive wear of non-doped corundum crystals versus wear directions and at the different sliding ratio; crystallographic plane (0001).

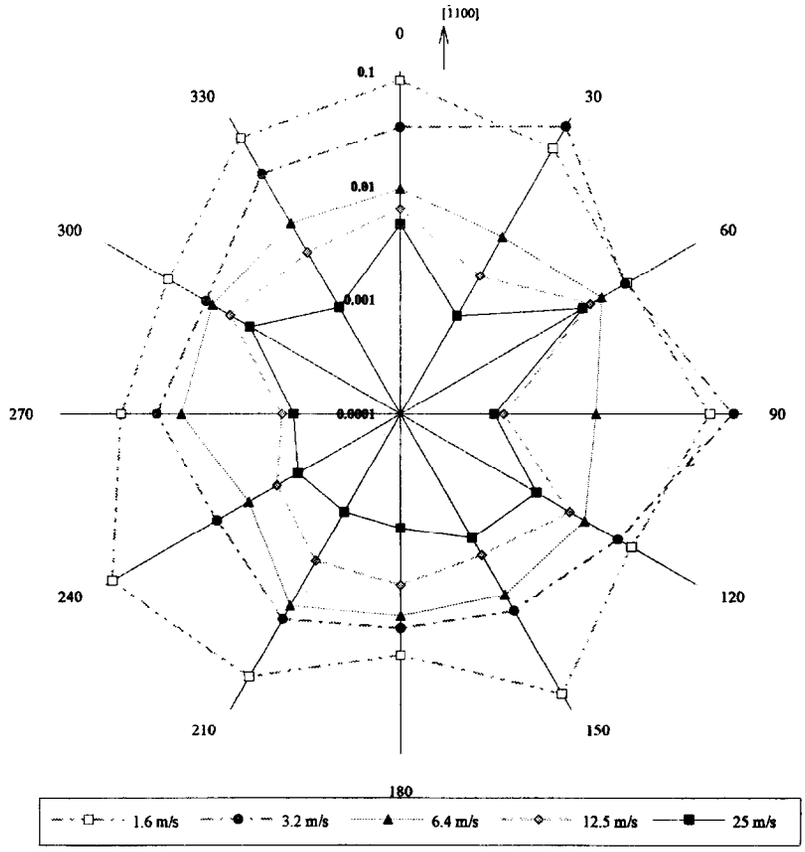

Fig. 6. Abrasive wear of non-doped corundum crystals versus wear directions and at the different sliding ratio; crystallographic plane{11$\bar{2}$0}.

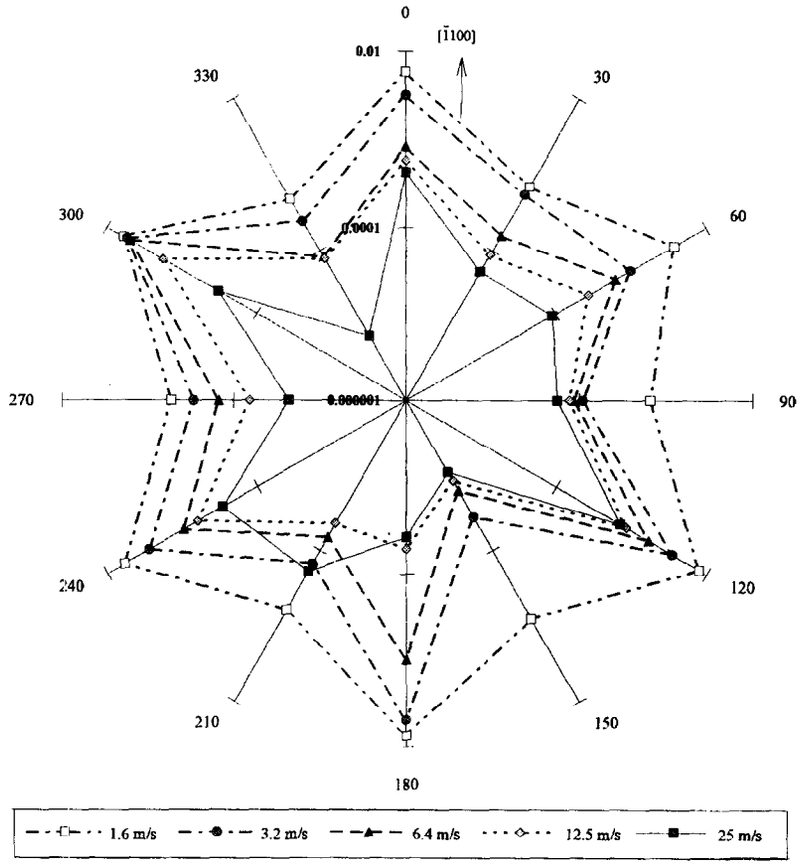

Fig. 7. Abrasive wear of Cr-doped (0·5 wt%) corundum crystals versus wear directions and at the different sliding ratio; crystallographic plane (0001).

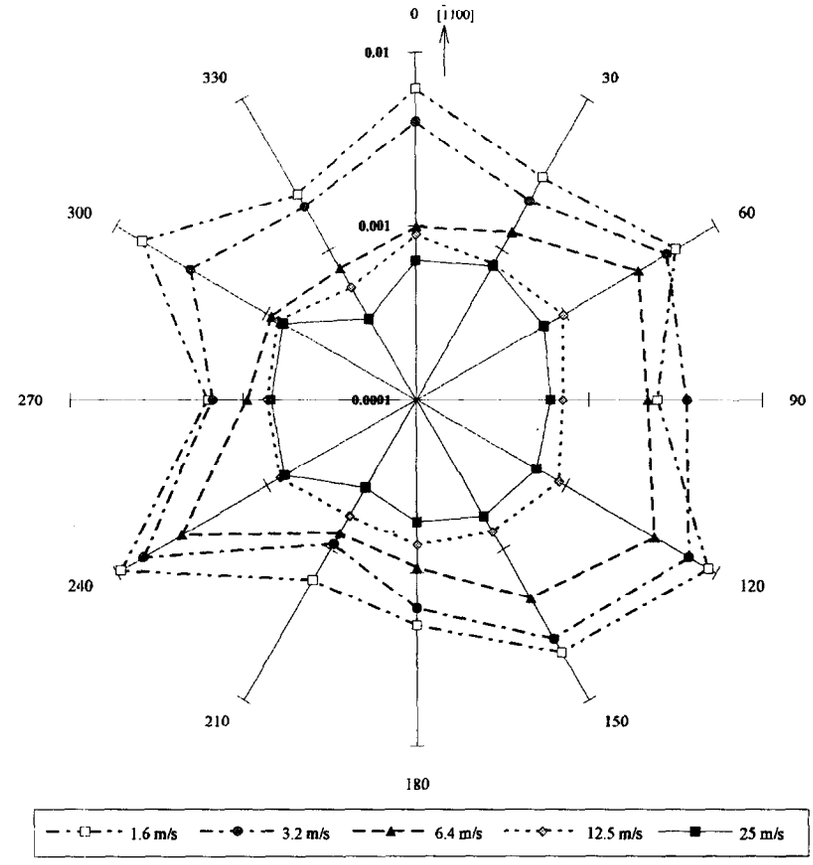

Fig. 8. Abrasive wear of Cr-doped (0·5 wt%) corundum crystals versus wear directions and at the different sliding ratio; crystallographic plane $\{11\bar{2}0\}$.

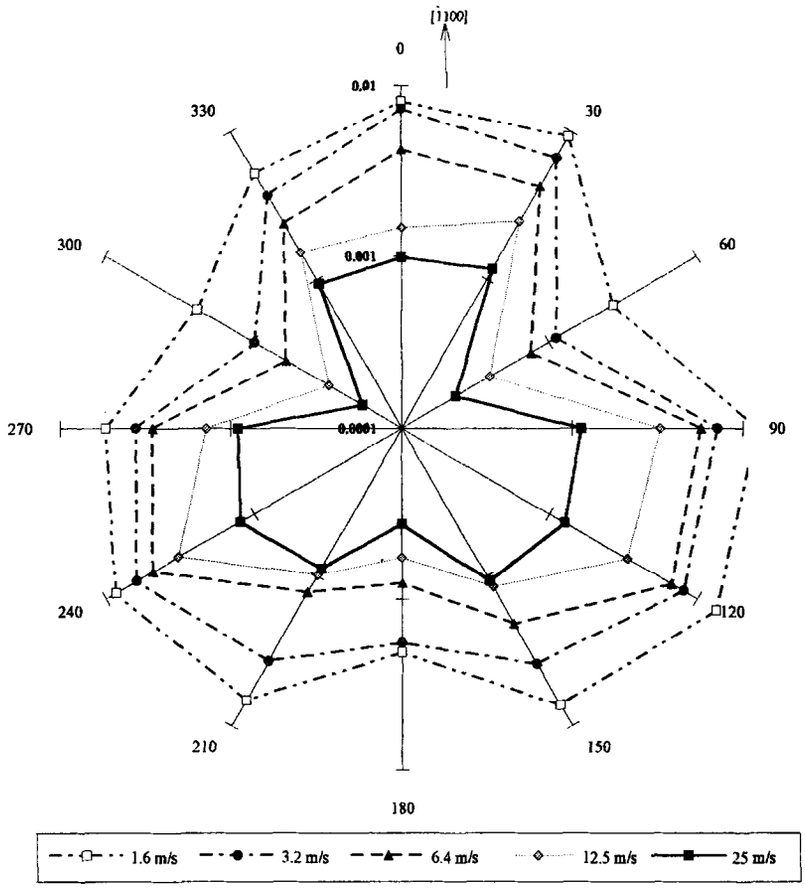

Fig. 9. Abrasive wear of Cr-doped (0·5 wt%) corundum crystals versus wear directions and at the different sliding ratio; crystallographic plane $\{11\bar{2}\cdot12\}$.

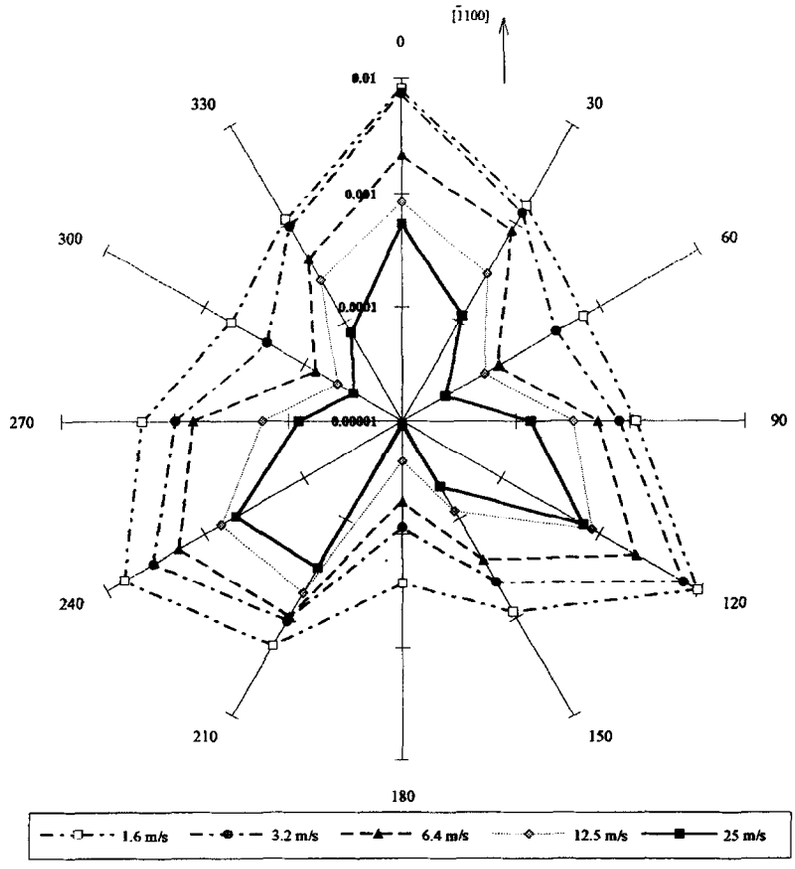

Fig. 10. Abrasive wear of Cr-doped (0·5 wt%) corundum crystals versus wear directions and at the different sliding ratio; crystallographic plane $\{11\bar{2}3\}$.

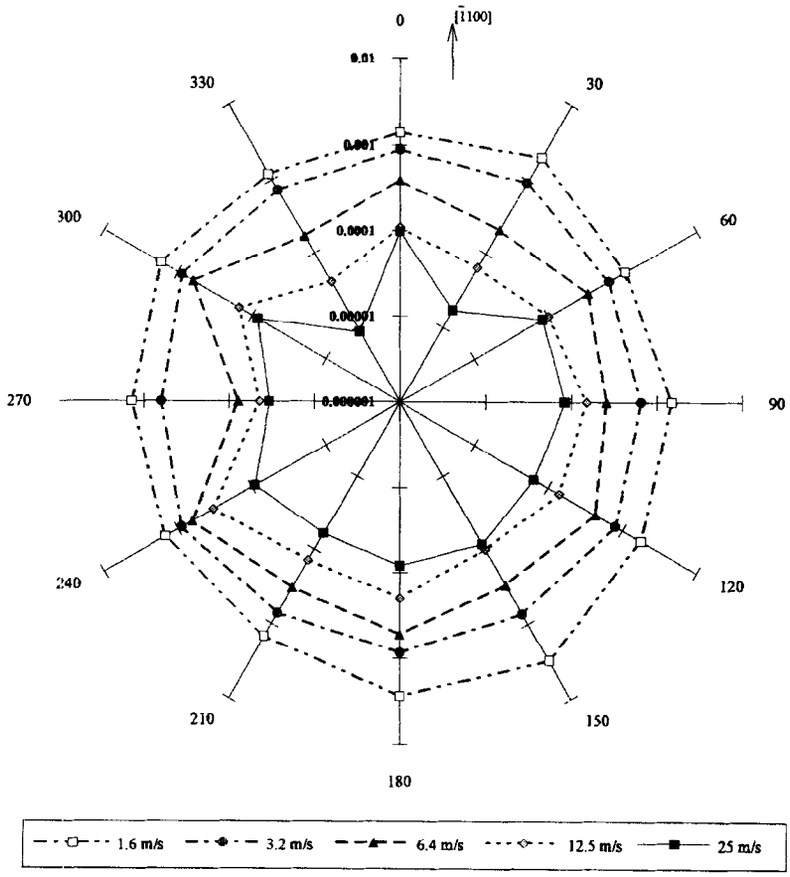

Fig. 11. Abrasive wear of Cr-doped (1·5 wt%) corundum crystals versus wear directions and at the different sliding ratio; crystallographic plane (0001).

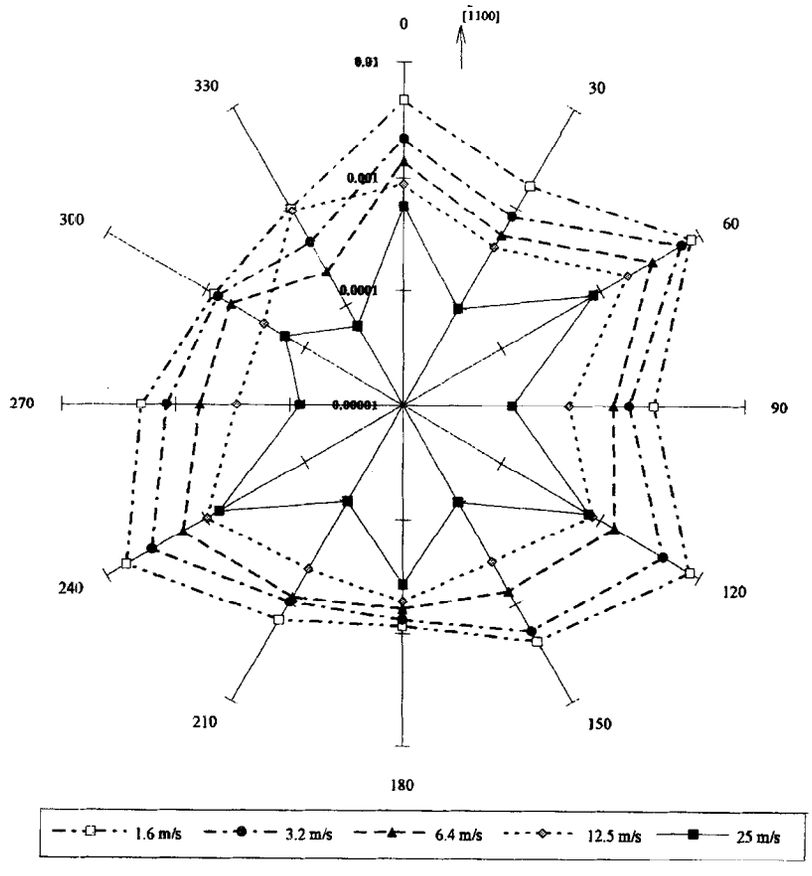

Fig. 12. Abrasive wear of Cr-doped (1·5 wt%) corundum crystals versus wear directions and at the different sliding ratio; crystallographic plane $\{11\bar{2}0\}$.

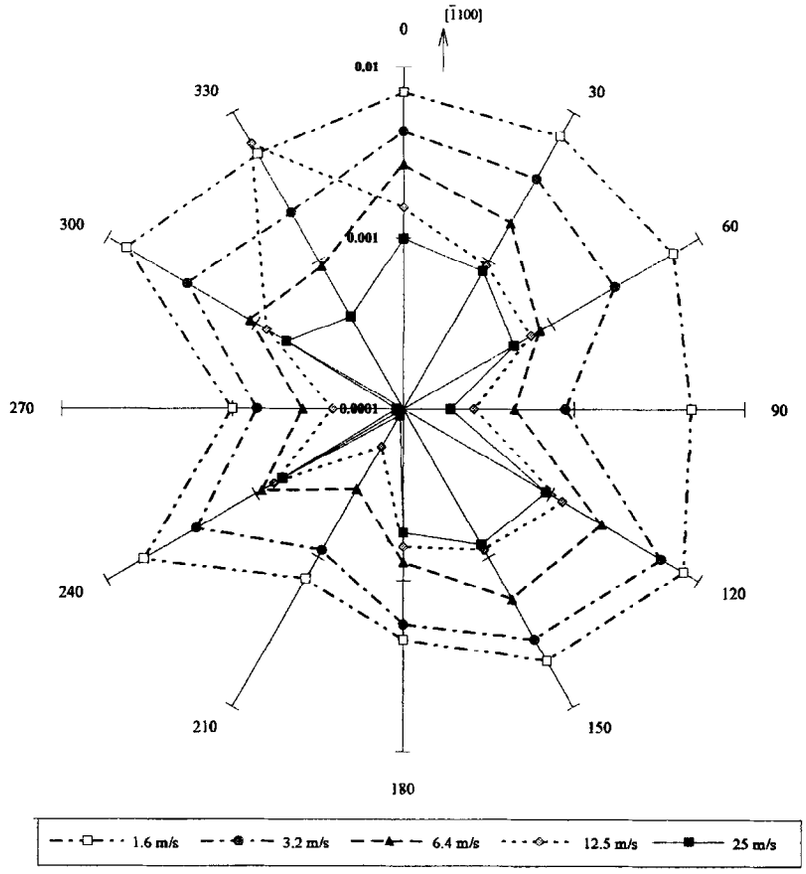

Fig. 13. Abrasive wear of Ti-doped (0·5 wt%) corundum crystals versus wear directions and at the different sliding ratio; crystallographic plane (0001).

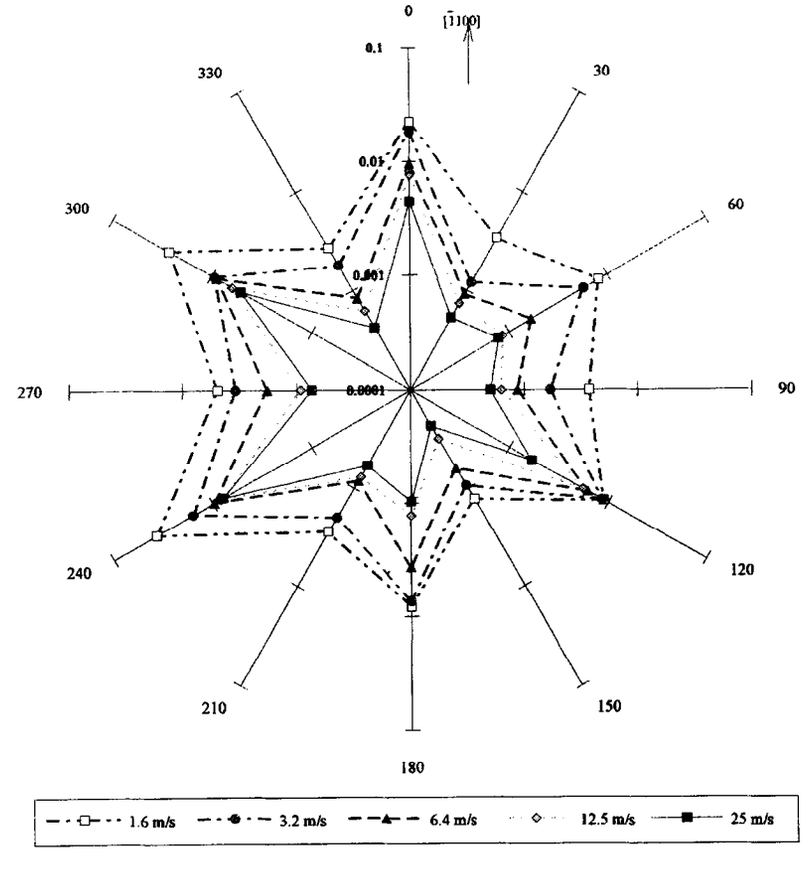

Fig. 14. Abrasive wear of Ti-doped (0·1 wt%) corundum crystals versus wear directions and at the different sliding ratio; crystallographic plane $\{11\bar{2}0\}$.

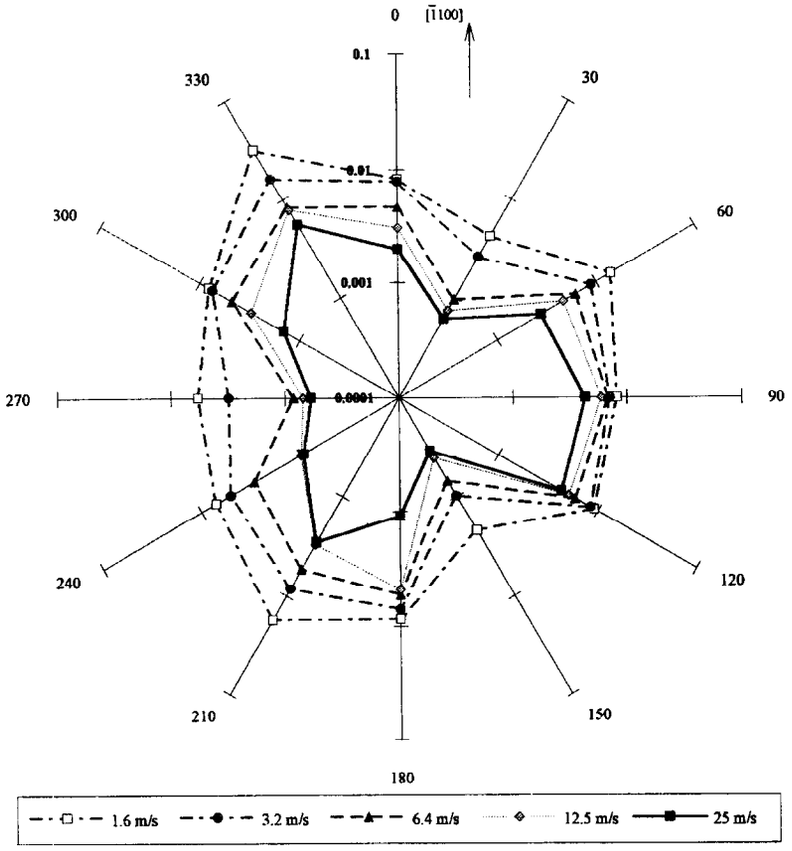

Fig. 15. Abrasive wear of Ti-doped (0·5 wt%) corundum crystals versus wear directions and at the different sliding ratio; crystallographic plane $\{11\bar{2}\cdot 12\}$.

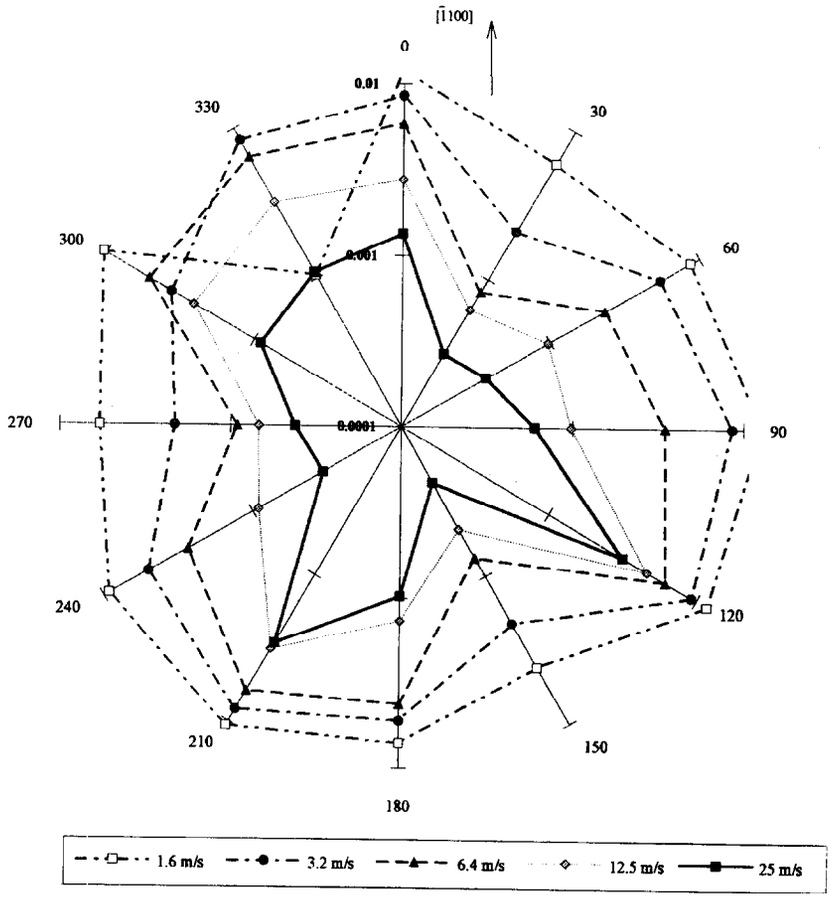

Fig. 16. Abrasive wear of Ti-doped (0·5 wt%) corundum crystals versus wear directions and at the different sliding ratio; crystallographic plane $\{11\bar{2}3\}$.

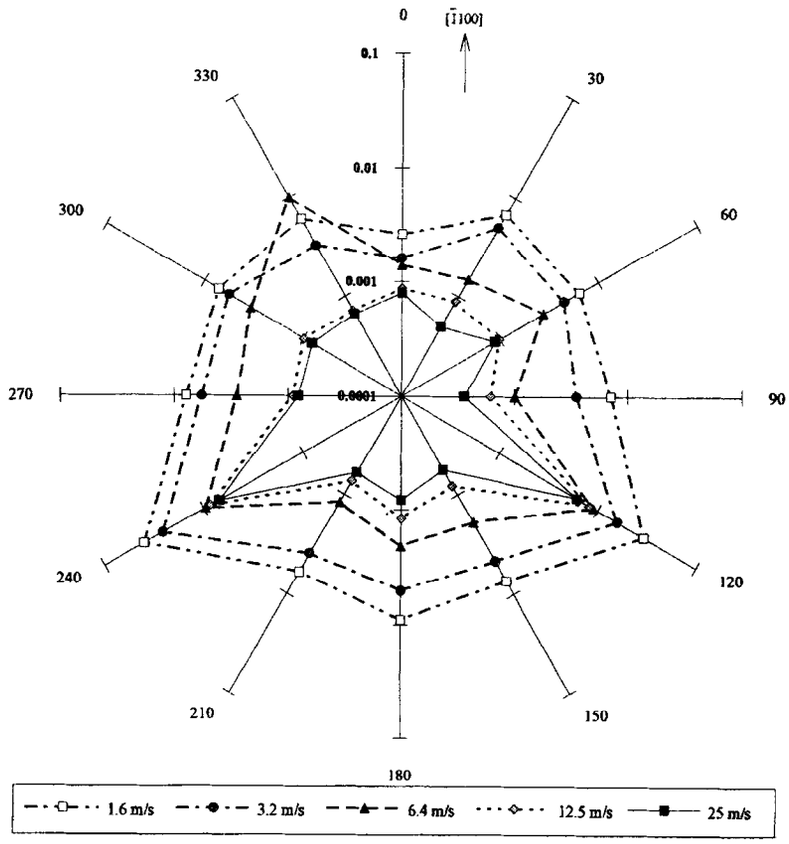

Fig. 17. Abrasive wear of Ti-doped (0·25 wt%) corundum crystals versus wear directions and at the different sliding ratio; crystallographic plane (0001).

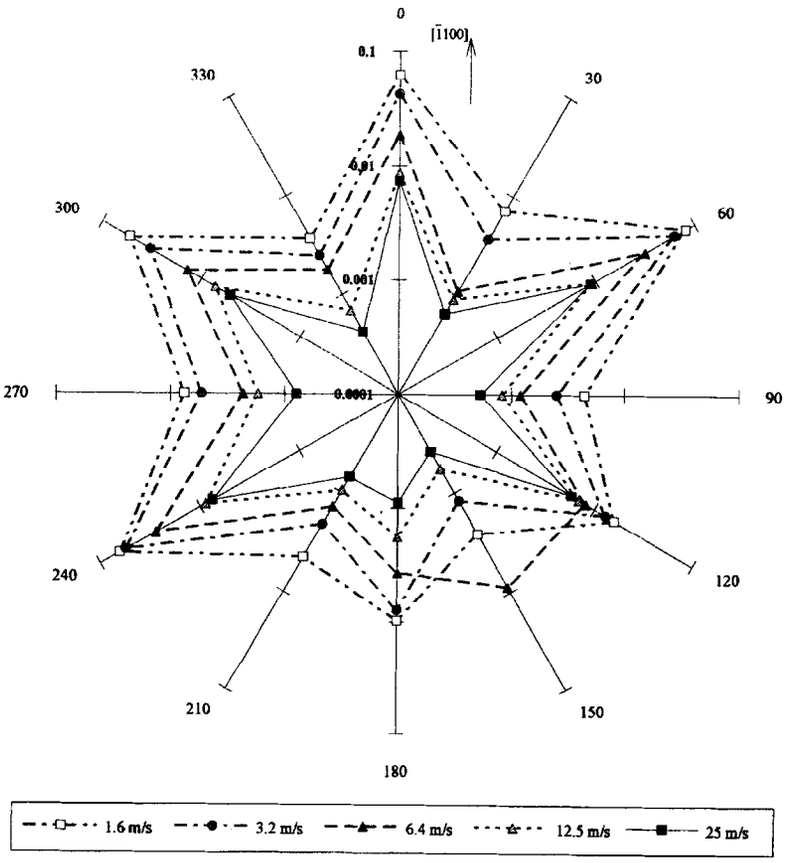

Fig. 18. Abrasive wear of Ti-doped (0·25 wt%) corundum crystals versus wear directions and at the different sliding ratio; crystallographic plane {11$\bar{2}$0}.

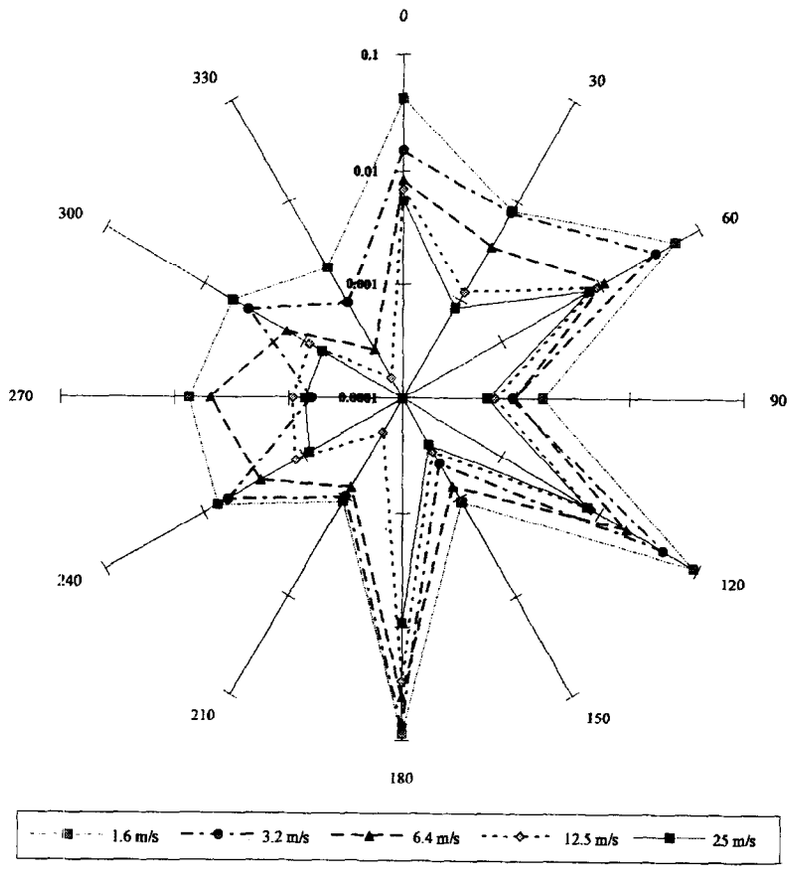

Fig. 19. Abrasive wear of Co-doped (0·1 wt%) corundum crystals versus wear directions and at the different sliding ratio; crystallographic plane (0001).

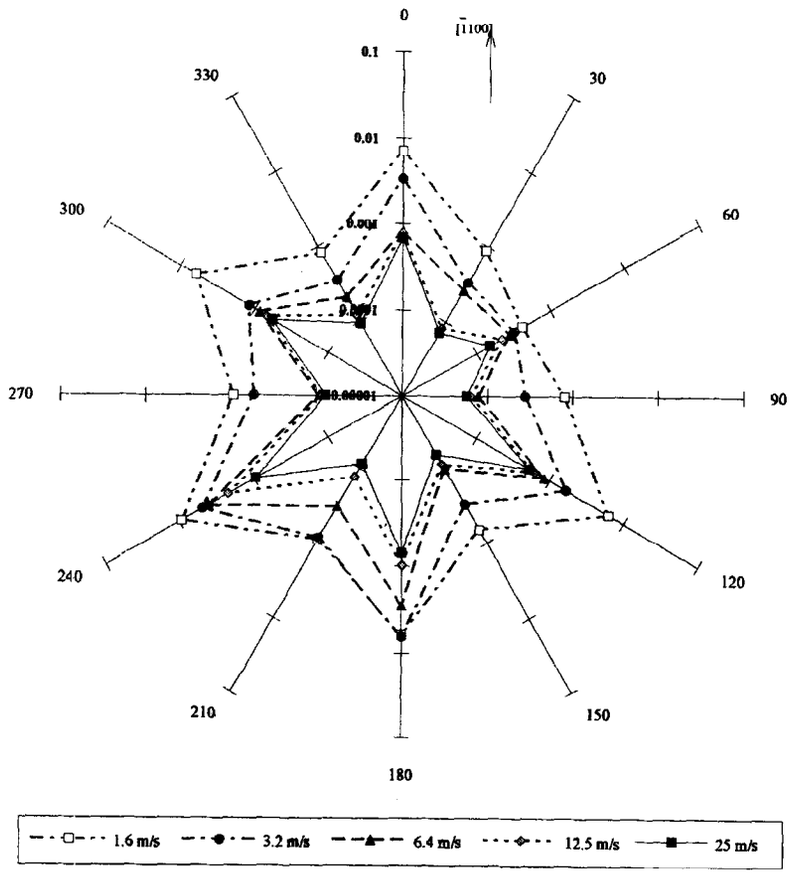

Fig. 20. Abrasive wear of Co-doped (0·1 wt%) corundum crystals versus wear directions and at the different sliding ratio; crystallographic plane $\{11\bar{2}0\}$.

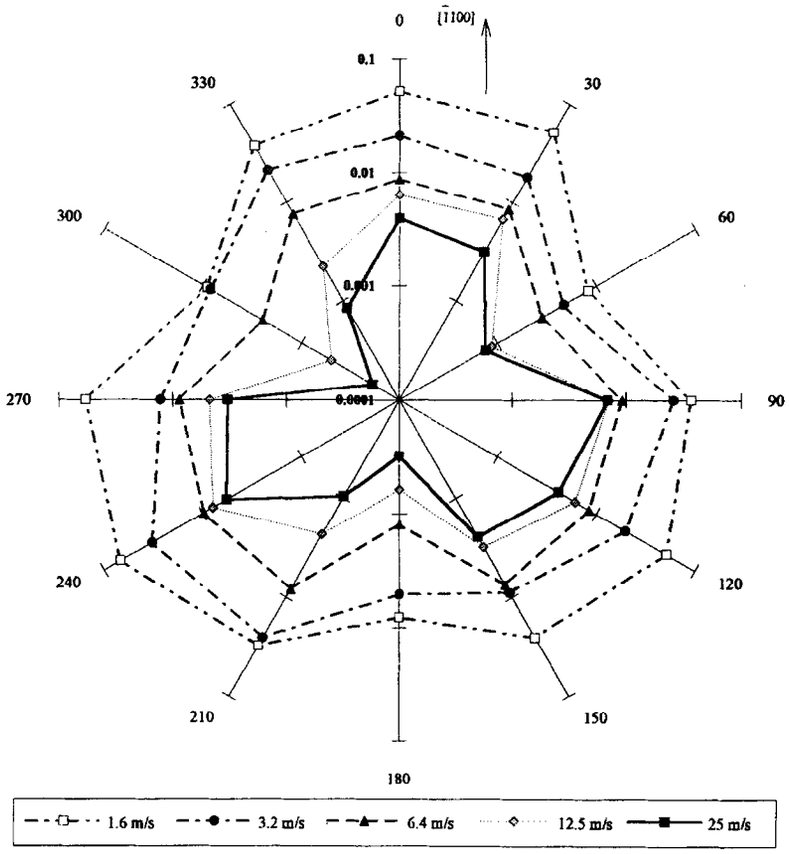

Fig. 21. Abrasive wear of Co-doped (0·1 wt%) corundum crystals versus wear directions and at the different sliding ratio; crystallographic plane $\{11\bar{2} \cdot 12\}$.

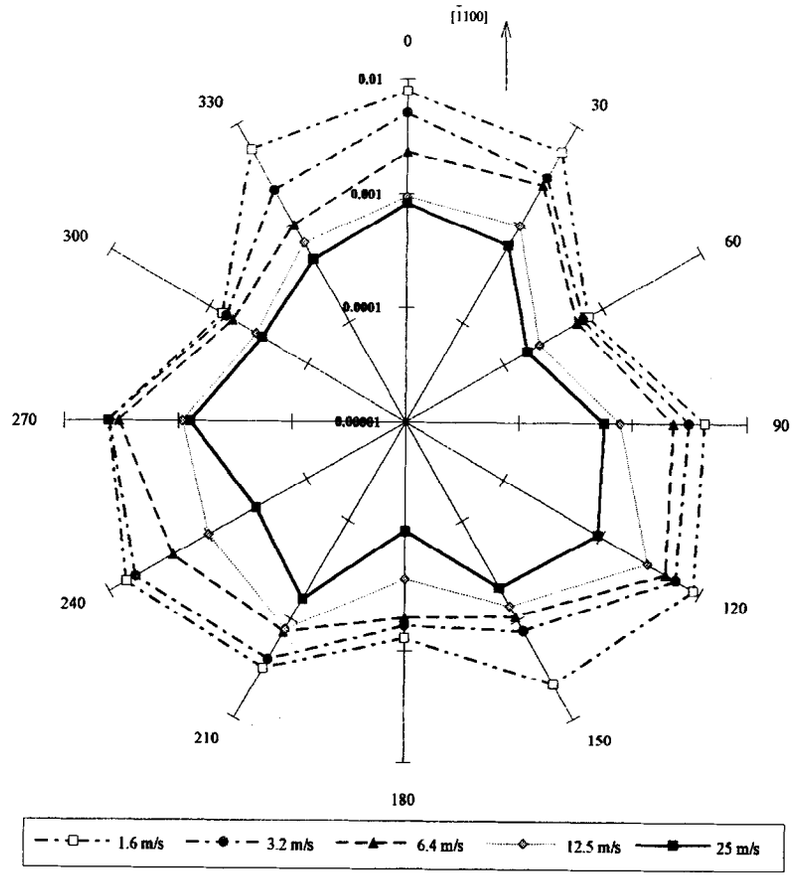

Fig. 22. Abrasive wear of Co-doped (0·1 wt%) corundum crystals versus wear directions and at the different sliding ratio; crystallographic plane $\{11\bar{2}3\}$.

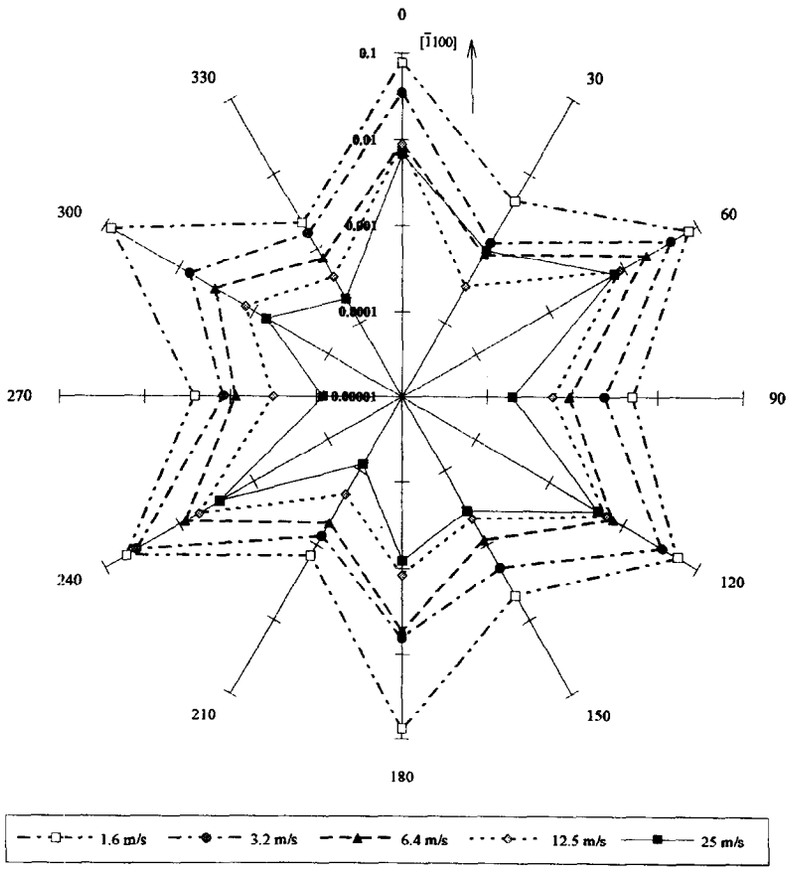

Fig. 23. Abrasive wear of Co-doped (0·5 wt%) corundum crystals versus wear directions and at the different sliding ratio; crystallographic plane (0001).

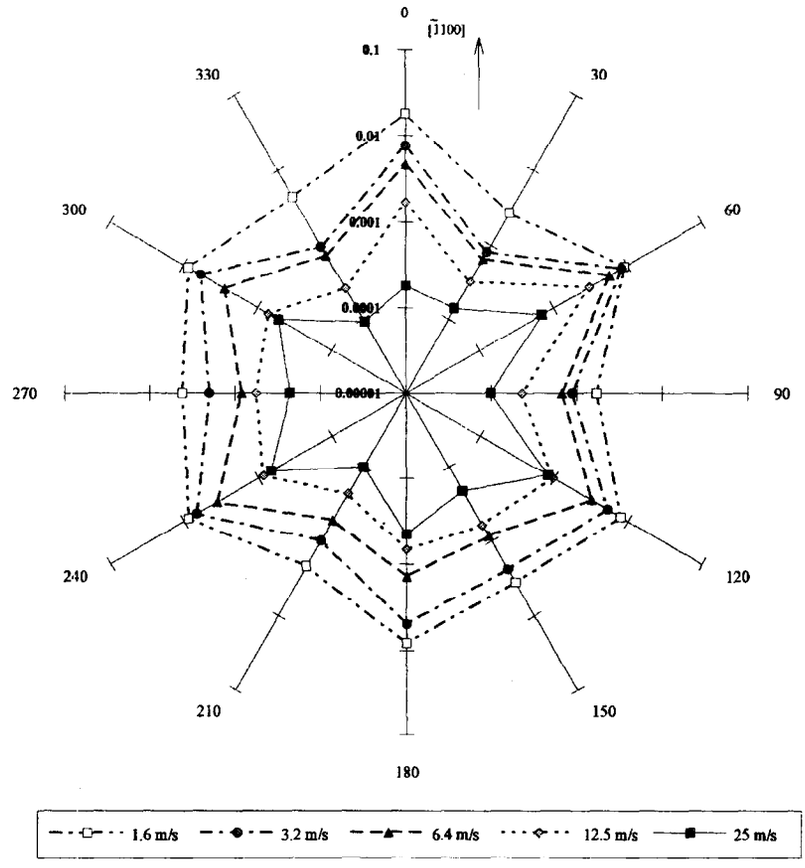

Fig. 24. Abrasive wear of Co-doped (0·5 wt%) corundum crystals versus wear directions and at the different sliding ratio; crystallographic plane {11$\bar{2}$0}.

References

1. Alford, W. J. and Stephens, D. L., *Journal Amer. Cer. Soc.*, 1963, **46** (4), 193.
2. Aulaytner, J., Rentgenowskie metody badań mozaiki i dyslokacji w kryształach, PWN, Warszawa.
3. Barański, W. T., Dabrowski, M. and Gawlik, J., Wybrane zagadnienia z konstrukcji i eksploatacji narzedzi skrawajacej w obróbce zautomatyzowanej, Poltechnika Krakowska, Krakó 1981.
4. Bastius. H., Berichte D. K. G., 62 (6/7) (1985), 53.
5. Becher, P. F., *Journal Amer. Cer. Soc.*, 1976, **59** (1/2), 59.
6. Becher, P. F., *Journal Amer. Cer. Soc.*, 1976, **59** (3/4), 143.
7. Blanchin, M. G., Castaing, G., Fontain, G., Heuer, A. H., Hobbs, L. W. and Mitchel, T. E., *Journal de Phys.*, 1981, **42** (3–1), 8.
8. Bojarskaja, J. S., Sztinca, Kiszyniev 1972.
9. Borkowski, J., Badanie własności skrawnych narzędzi ściernych Materiały Konferencyjne Technologia Obróbki Ściernej, SIMP Rzeszów 1974.
10. Borkowski, J., Elementarne zjawiska zużycia ziarn i narzędzi ściernych, WSI Koszalin 1983.
11. Castaing, J., Cadoz, J. and Kirby, S. H., *Journal de Phys.*, 1981, **42** (6), 42.
12. Catlow, C. R. A., James, R., Mackrodt, S. H. and Steward, R. F., *Phys. Rev.*, 1982, **B25**, 1006.
13. Conrad, H., Janowski, K. and Stofel, E., *Trans AIME*, 1965, **233** (1), 253.
14. Cottrell, A. H., *Theory of Cristal Dislocation*, London, 1964.
15. Dereń. J., Haber, J., Pampuch, R. Chemia ciała stałego, PWN Warszawa, 1973.
16. Draper, N. R. and Smith, J. P., Analiza regresji stosowana, PWN Warszawa 1973.
17. Dutt, B. V, Hurrel, J. P. and Kroger, F. A., *Journal Amer. Cer. Soc.*, 1975, **58** (9/10), 420.
18. Dutt, B. V. and Kroger, F. A., *Journal Amer. Cer. Soc.*, 1975, **58** (1112), 474.
19. Eiss, N. S., *Trans. ASME*, 1967, **89B** (3), 463.
20. Gościńska, T. Ph. D. thesis, AGH Kraków, 1976.
21. Howitt, D. G. and Mitchel, T. E., *Phil. Mag.*, 1981, **A44**, 229.
22. Hwang, L., Heuer, A. H. and Mitchel, T. E., *Deformation of Ceramics Materials*, Plenum Press, New York, 1975.
23. Kelly, A., Krystalografia i defekty kryształów, PWN Warszawa 1980.
24. Lal, G. K., Matsuo, T. and Shaw, M. C., *Wear*, 1973, **24** (3), 279.
25. Nedoma, J. (ed.), *Elementy symetrii, grupy punktowe*, University of Mining and Metallurgy, Kraków 1984.
26. Nedoma, J., Kasprzyk, W. and Schreiner, P., *Interpretacja Lauegramów, Parts I, III and VI*, University of Mining and Metallurgy, Kraków 1981.
27. Nye, J. F., Własności fizyczne kryształów, PWN Warszawa 1987.
28. Oczoś, K., Analiza procesu i metody pomiaru zużycia pojedynczych ziarn ściernych i ściernic, Politechnika Rzaszów, 1975.
29. Pampuch, R., Haberko, K., Kordek, M.
30. Peckner, D., *The strengthening of metals*, Reinhold Publication Co., New York, 1964.
31. Pletka, B. J., Mitchell, T. E. and Heuer, A. H., *Phys. Stat. Sol.*, 1977, **39**, 301.
32. Pletka, B. J., Mitchell, T. E. and Heuer, A. H., *Acta crystall.*, 1982, **30**, 147.
33. Toh, S. B. and McPherson, R., *Mater. Science Res.*, 1984, **18**, 723.
34. Woźniak, K., Nowe materiały ścierne, Politechnika Koszalińska, Koszalin 1985.
35. Willey, J. (ed.), *Crystal technology*, New York 1976.